

www.acsabm.org Article

DFMO Carbon Dots for Treatment of Neuroblastoma and Bioimaging

Suraj Paudyal, [▽] Frederic Anthony Vallejo, [▽] Emel Kirbas Cilingir, Yiqun Zhou, Keenan J. Mintz, Yelena Pressman, Jun Gu, Steven Vanni, Regina M. Graham,* and Roger M. Leblanc*



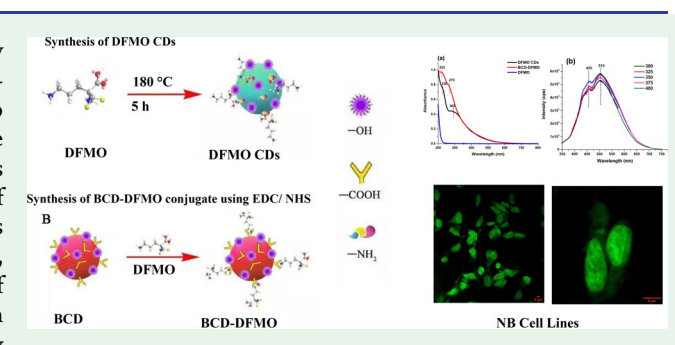
Cite This: ACS Appl. Bio Mater. 2022, 5, 3300-3309



ACCESS

III Metrics & More

ABSTRACT: Neuroblastoma (NB) is a pediatric malignancy affecting the peripheral nervous system. Despite recent advancements in treatment, many children affected with NB continue to submit to this illness, and new therapeutic strategies are desperately needed. In recent years, studies of carbon dots (CDs) as nanocarriers have mostly focused on the delivery of anticancer agents because of their biocompatibility, good aqueous dissolution, and photostability. Their fluorescence properties, surface functionalities, and surface charges differ on the basis of the type of precursors used and the synthetic approach implemented. At present, most CDs are used as nanocarriers by



Article Recommendations

directly linking them either covalently or electrostatically to drug molecules. Though most modern CDs are synthesized from large carbon macromolecules and conjugated to anticancerous drugs, constructing CDs from the anticancerous drugs and precursors themselves to increase antitumoral activity requires further investigation. Herein, CDs were synthesized using difluoromethylornithine (DFMO), an irreversible ornithine decarboxylase inhibitor commonly used in high-risk neuroblastoma treatment regiments. In this study, NB cell lines, SMS-KCNR and SK-N-AS, were treated with DFMO, the newly synthesized DFMO CDs, and conventional DFMO conjugated to black carbon dots. Bioimaging was done to determine the cellular localization of a fluorescent drug over time. The mobility of DNA mixed with DFMO CDs was evaluated by gel electrophoresis. DFMO CDs were effectively synthesized from DFMO precursor and characterized using spectroscopic methods. The DFMO CDs effectively reduced cell viability with increasing dose. The effects were dramatic in the N-MYC-amplified line SMS-KCNR at 500 μ M, which is comparable to high doses of conventional DFMO at a 60-fold lower concentration. In vitro bioimaging as well as DNA electrophoresis showed that synthesized DFMO CDs were able to enter the nucleus of neuroblastoma cells and neuronal cells and interact with DNA. Our new DFMO CDs exhibit a robust advantage over conventional DFMO because they induce comparable reductions in viability at a dramatically lower concentration.

KEYWORDS: carbon dots, DFMO, neuroblastoma, bioimaging, anticancer, nanoparticle

1. INTRODUCTION

Neuroblastoma (NB) is a pediatric tumor of the autonomic nervous system that develops in the adrenal medulla, and its lesions commonly develop around the abdomen, neck, chest, and spine region. NB accounts for about 8–10% of all childhood cancer and 15% of deaths from pediatric tumors. Several molecular drivers of neuroblastoma have been identified, notably N-MYC amplification, which results in exceptionally aggressive tumors carrying poor prognoses. N-MYC is a class of proto-oncogene protein that is encoded by the MYCN gene, which promotes the expression of many ribosomal genes involved in cell growth, differentiation, and apoptosis. Amplification of the MYCN gene can cause overexpression of proto-oncogene N-MYCN, which can cause unscheduled DNA replication and the formation of extrachromosomal DNA that results in unhindered and excessive cell proliferation. It has been

found that N-MYC amplification is one of the determining factors in NB and in most cases classified as aggressive or stage 4 tumor. Despite intensive multimodal treatments, many patients develop aggressive, relapsing metastatic disease. Moreover, chemotherapies used at maximal tolerated doses have long-term adverse effects that include cognitive and developmental deficits, as well as increased risks of additional cancers in the future. Therefore, there exists a clear need for safer, more efficacious, and precisely targeted therapies.

Received: April 3, 2022 Accepted: June 13, 2022 Published: June 30, 2022





DFMO is an irreversible inhibitor of ornithine decarboxylase (ODC) enzyme. The enzyme is typically upregulated in neuroblastoma, downstream of N-MYC amplification, and is the rate-limiting enzyme in polyamine biosynthesis. DFMO is specially effective in patients with high-risk neuroblastoma.⁶ Current trials on DFMO use in pediatric NB patients include a lower dose of DFMO alone (2000 mg/m²/day) as standard therapy, as well as a high dose of DFMO (up to 9000 mg/m²/ day) alongside other chemotherapeutic drugs. The most common side effects of the high dose of DFMO are hematologic-like anemia (low red blood cells count, 40%), leukopenia (low white blood cells count, 20-30%), and thrombocytopenia (low platelet count, 50%). Other side effects include seizures, because of higher concentrations in cerebrospinal fluid, and osmotic diarrhea when given orally. Despite the drastic improvements in NB treatments over the last several decades, innovative therapeutic strategies are necessary for children with high-risk disease.

Carbon dots (CDs) are carbon-based spherical nanoparticles with luminescent properties and sizes of less than 10 nm. They possess high photostability, tunable emission, low molecular weight, and high-water solubility, thus meeting the requirements of optical imaging agents. In recent years, metal-based NPs have received increasing interest in medical and industrial applications; however, their toxicity and bioincompatibility has also been demonstrated. Cadmium-based QDs like cadmium telluride quantum dots (CdTe-QDs) and cadmium selenide (CdSe) quantum dots are mostly studied for fluorescent probes as therapeutic carriers for tissue imaging. However, they have demonstrated liver and kidney toxicity, mostly because of oxidative stress and through consumption of endogenous antioxidants. Moreover, they also show cellular apoptosis, mitochondrial destruction, and imbalance in intracellular ions signaling. 10 Similarly, use of gold nanoparticles had been widespread for a time because of their simple synthesis methods and ease of conjugation with peptides, DNA, and antibodies. However, some studies have shown that these gold nanoparticles can be retained in the biological system and can cause oxidative DNA damage and downregulate cell cycle genes.¹¹ Silica nanoparticles have widespread applications in industrial sectors, such as the fabrication of electric and thermal insulators, but a comprehensive study suggested that exposure to silica nanoparticles (1-100 nm) induced toxicity in mammalian cell lines and mice. 12 CDs have considerable advantages over both metallic quantum dots and other dye-based organic nanodots in the field of bioimaging. CDs have been used successfully for both in vitro and in vivo cell imaging without necessitating further functionalization. Recently, CDs have gained attention as nanocarriers because of their tunable surface functionality, which allows for drug conjugation without the need for additional linkers.

Theranostic approaches in oncologic treatment, in which therapies are designed with both diagnostic and therapeutic functionality, have been gaining popularity during the past decade. In contrast to CDs, nanoparticle-based theranostic agents such metal quantum dots and silica and gold nanoparticles have been extensively studied. These agents can be implemented as tools in fluorescence imaging, MRI contrast agents, and X-ray computed tomography (CT scan) with integrated radiation therapy, chemotherapy, and photothermal therapy. However, many traditionally utilized nanoparticles often have problems related to poor biocompatibility, low water solubility, and poor elimination from the body. In the solution of the body.

CDs, in contrast, do not pose these obstacles and provide an excellent advantage because they can be used simultaneously for fluorescent imaging as well as for drug delivery as nanocarriers. ^{23,24}

Up to now, CDs have been synthesized using a variety of precursors like small molecules, natural and synthetic polymers, polysaccharides, proteins, and bioresources from plants or animals. Photoluminescence properties, surface functionalities, surface charge, and potential functional groups on the CD surface vary depending upon the precursors and synthesis modality used. Most CDs are used as nanocarriers by directly linking them covalently or electrostatically with active ingredients. Therefore, if a conventional therapeutic agent is used as a precursor for synthesis, there is a chance of developing CDs with active moieties exposed as functional groups on their surface. Thus, CDs synthesized from DFMO may retain properties not only of traditional CDs but also also of conventional therapeutic DFMO, such as anti-NB potential. Herein, difluoromethylornithine (DFMO), a drug used in neuroblastoma (NB) refractory to treatment, has been selected to synthesize CDs.

In an effort to increase therapeutic efficacy as well as reduce the required dosage and toxicity, our group synthesized new DFMO CDs from traditionally used DFMO. The newly synthesized DFMO CDs were treated with neuroblastoma cell lines, SMS-KCNR and SK-N-AS. These cells lines were particularly chosen because they are N-MYC-amplified cell lines and are aggressive forms of tumors with a higher prevalence among NB cases. Additionally, we investigated the photoluminescence (PL) properties and biodistribution of our DFMO CDs for use as a potential imaging modality. Our new CDs developed from DFMO drug as a precursor may carry therapeutic potential both as a treatment modality and as an imaging agent in the future.

2. EXPERIMENTAL SECTION

Supplies. DFMO drug (purity ≥97%) was purchased from Sigma Aldrich. Millipore Direct-Q 3 (Type1) water was used throughout the experiment. A dialysis bag from VWR (West Chester, PA) of 100–500 Da molecular weight cutoff (MWCO) and dialysis tubing with MWCO of 3500 Da from Thermo Scientific was used.

Synthesis of DFMO CDs. DFMO (5g) was dissolved in 50 mL of water and was ultrasonicated until it dissolved completely. This was transferred to a 75 mL Teflon tube and subjected to thermal treatment at 180 °C for 5 h. After bringing the autoclave to room temperature, crude DFMO carbon dot solution was obtained. This was centrifuged (3000 rpm, 30 min), and any precipitates were removed. The solution was then dialyzed using a 500 Da MWCO dialysis bag with 4 L of DI water for 3 days. Then, the resultant solution was concentrated using a rotavapor until about 10 mL remained. After that, the solution was subjected to freeze-drying to obtain solid carbon dots of \approx 30 mg.

Synthesis of Black CDs and DFMO Conjugate (BCD-DFMO). Ten mg of BCDs was dissolved in 6 mL of phosphate buffer solution (PBS, 7.4 pH). Then, 20 mg of 1-(3-(dimethylamino)propyl)-3-ethylcarbodiimide hydrochloride (EDC) solubilized in 1 mL of PBS was added to the prepared BCDs solution. This was continuously mixed at 20.0 \pm 1.0 °C for 30 min. Then 15 mg of *N*-hydroxysuccinimide (NHS) mixed in 1 mL of PBS was added. After 30 min of mixing, 20 mg of DFMO dissolved in 1 mL of PBS was added. The final solution was stirred at 20.0 \pm 1.0 °C overnight. The resultant solution was dialyzed with a dialysis bag of 3500 MWCO for 3 days, and the water was changed every 6–12 h. The final solution was kept at –80 °C and then subjected to a lyophilizer to obtain a brown, powdered product.

Characterization of DFMO CDs. The prepared carbon dots were studied using UV-vis (1 cm cell quartz cuvette) in a Cary 100 UV-vis spectrophotometer (Agilent Technologies) in DI water. The fluorescence spectra of the DFMO CDs were measured in a 1 cm

ACS Applied Bio Materials www.acsabm.org Article

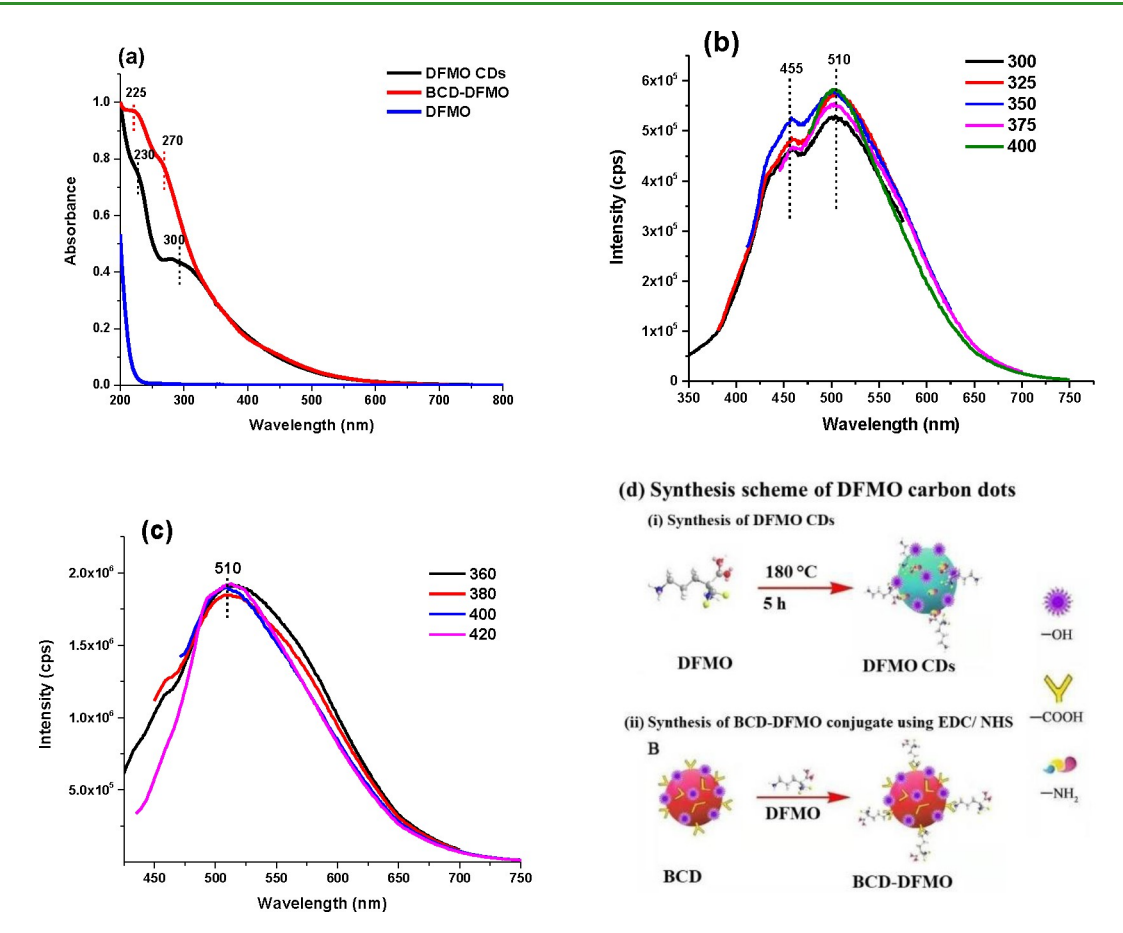


Figure 1. (a) UV—vis absorption spectra of DFMO, DFMO CDs, and BCD-DFMO. The samples $(10 \,\mu g \, ml^{-1})$ were used in a 1 cm quartz cell (slit width of 5 nm). PL emission spectra of (b) DFMO CDs and (c) BCD-DFMO. (d) Synthesis scheme of DFMO CDs.

path-length quartz cuvette using a Horiba Jobin Yvon Fluorolog-3 with a slit width of 5 nm for both excitation and emission wavelength. The Fourier transformation infrared (FTIR) spectrum was measured using the PerkinElmer Frontier ATR instrument. Atomic force microscopy was performed with an Agilent 5420 AFM (Agilent Technologies) using tapping mode, and transmission electron microscopy (TEM) was performed using a JEOL 1200× TEM. The zeta potential of the DFMO CDs was measured with the Malvern Zetasizer (Westborough, MA). The elemental analysis was performed using a 2400 Series II CHNS/O Elemental Analyzer. The XRD patterns were collected with a Phillips X'pert Diffractometer that uses a copper source (0.154 nm wavelength). The lattice spacing d can be calculated from the Braggs condition: $2d\sin\theta = n\lambda$, where 2θ is the peak position in the XRD pattern.

Quantum Yield Calculations. The quantum yield (Φ) of asprepared DFMO CDs was calculated using the standard protocol used in our previous papers. ^{29,30}

Cell Culture and Reagents. The MYCN-amplified neuroblastoma cell line SMS-KCNR was provided by the Children's Oncology Group. The SK-N-AS (non-MYCN-amplified neuroblastoma cell line) was provided by the American Type Culture Collection (ATCC, Manassas, VA, USA). Our cell culture methods have previously been published. All cell lines including dissociated dorsal root ganglion (DRG) were cultured in the conditions mentioned in our previously published paper. 32

Immunocytochemistry. The purity and morphology of the resulting DRG neurons was confirmed by staining cells with mouse antineurofilament antibody (RT97; Developmental Studies Hydridoma Bank, Iowa City, IA). For cell fixation, 4% (PFA) paraformaldehyde was used, followed by washing with PBS. The cells were incubated using a blocking solution of 10% NGS mixed with 0.2% Triton X-100 for an hour at room temperature, followed by an overnight incubation with a 1:500 dilution of RT-97 antibody. Cells were washed again and

visualized using a 1:200 dilution of goat anti-mouse IgG conjugated to Alexa Fluor 594 (Invitrogen Grand Island, NY).

In Vitro Cytotoxicity Studies. The chemotherapeutic effects of DFMO, DFMO CDs, and BCD-DFMO conjugate were studied in pediatric neuroblastoma cell lines SK-N-AS and N-MYC-amplified SMS-KCNR. An MTS assay was conducted for cell viability studies. For this, the cultured cells were transferred into 96-well plates at 1.5×10^5 cells per well, 24 h prior to drug treatment. These cells were treated with 10, 100, or 500 μ M and 1, 10, or 30 mM of DFMO drug. Similarly, each cell line was also treated with 10, 100, and 500 μ M of DFMO CDs, as well as BCD-DFMO conjugate. The cells were incubated for 72 h, and viability was examined using the CellTiter 96 Aqueous One Solution Cell Proliferation Assay (Promega). The instructions for the assay were followed as given by the manufacturer, which is mentioned in our previously published paper. ²⁹ Different batches of the CDs were used to maintain the consistent data.

Statistical Analysis. Student's t tests were used for all pairwise comparisons of the data for cell viability tests and were presented as mean \pm SEM.

In Vitro Bioimaging. SK-N-AS and SMS-KCNR cell lines were grown on 24-well plates with coverslip (12 mm) at 1.5×10^5 cells per plate in RPMI media, which was incubated for 24 h for adequate cell growth for imaging. After that, only the media was aspirated out, and cells were treated with 1 mM of DFMO CDs resuspended in RPMI media and further incubated for 1, 8, and 24 h. The DRG neuronal cells were subjected to 1 mM DFMO CDs for 1 h. After the treatment was finished, PBS solution was used to wash the cells, which were treated with 4% PFA for 30 min before final washing with PBS again. The coverslip was carefully removed, inverted, and placed on a microscope slide with antifade mounting media (Thermo Fisher Scientific, Waltham, MA). The DRG neuronal cells were imaged directly through the 24-well plates. Confocal images were taken with the EVOS FLoid

Imaging System (Thermo Fisher Scientific, Waltham, MA) or the Leica SP5 confocal microscope (Leica Microsystems Inc., Buffalo Grove, IL).

DNA Mobility Assay. The motility of DNA mixed with DFMO CDs was evaluated by gel electrophoresis to determine if DFMO CDs interact with DNA. Increasing concentrations (1–1000 mM) of DFMO CDs were mixed with either a 265 (mouse) or 1362 (rat) bp DNA solution (10 μ g) and subjected to agarose gel (3% and 1.5%, respectively) electrophoresis in the presence of ethidium bromide for 100 min. Images were taken using a ChemiDoc imaging system (Bio-Rad).

3. RESULTS

Characterization of DFMO, DFMO CDs, and BCD-DFMO. DFMO CDs were prepared by a "bottom-up" approach using DFMO as a precursor. Final product CDs were aqueous soluble. Spectroscopic techniques were utilized to characterize the CDs. Figure 1a shows the UV-vis spectrum of the three compounds DFMO, DFMO CDs, and BCD-DFMO with water as a solvent. The absorption band at 230 nm for DFMO CDs and 225 nm for BCD-DFMO can be assigned to a $\pi-\pi^*$ electronic transition of fundamental C=C groups present in most CDs. Furthermore, the 300 nm band for DFMO CDs and 270 nm for BCD-DFMO can be attributed to an $n-\pi^*$ transition of C=O functional groups present in the compounds. 33,34 The DFMO precursor drug itself does not have any absorption in the UV-vis region.

The synthesized DFMO CDs have excitation-independent PL and display emission maxima at 455 and 500 nm while exciting from 300 to 400 nm (Figure 1b). The PL emission maximum is at both 455 and 505 nm when excited at 350 nm. Similarly, PL of BCD-DFMO conjugate (Figure 1c) showed an excitationindependent emission at 510 nm when excited at different wavelengths with an excitation maximum at 360 nm. The mechanism behind the excitation-independent PL is commonly attributed to the surface functionalities and monodispersed particles. 35,36 The PL emission maximum is at 455 and 505 nm when excited from 300 to 400 nm. This can be explained through the presence of two emissive states: one carbon core with an sp² carbon network and another molecular state with fluorophorelike moieties. Since only one molecule of DFMO was used as a precursor, and the purification step involved use of a dialysis bag, monodispersed CDs were obtained, which led to excitation-independent PL. The DFMO drug, itself, does not show any PL since it does not have any fluorophore group.

The quantum yield (QY) of CDs is accepted as one of the most important characteristics to be known because CDs have been employed for various biomedical applications because of low toxicity and superior photoluminescence properties.³ There are key points for the QY calculations to be performed for at least 3 repetitions for consistent experimental setups. Here, we chose quinine sulfate and harmane as our standards because they possess overlap with the emission range of DFMO CDs. Furthermore, cross-calibration of two standards was also performed before starting the QY calculation of the sample. We have observed that the QY yields of quinine sulfate (literature Φ = 54%) and harmane (literature Φ = 83%) were 55 and 81.5%, respectively, according to our experimental setup. Therefore, we can be assured that our methodology was reliable with minor deviations. Following the results, we measured the QY of the DFMO CDs by proceeding with the same protocol. Finally, the QY of DFMO CDs was calculated as 1.8%.

FTIR-ATR spectroscopy for each compound, in solid state, was measured to indicate the functional groups present (Figure 2). The DFMO CDs showed broad vibration bands between

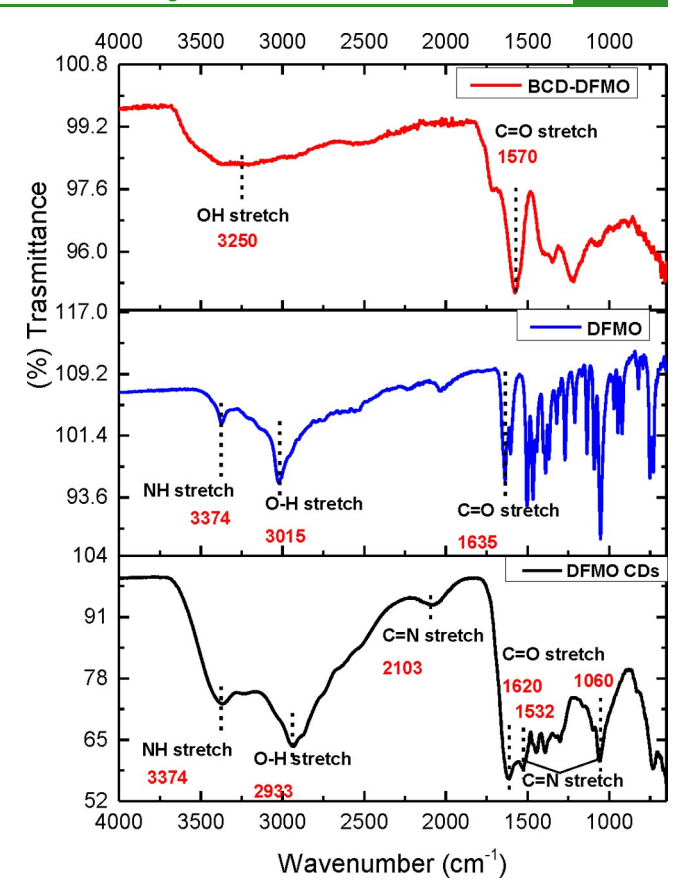


Figure 2. FTIR-ATR spectra of BCD-DFMO conjugate, DFMO, and DFMO CDs.

3000 and 3500 cm⁻¹, which can be attributed to O-H and N-H stretching vibrations. The O-H stretch peak at 2933 cm⁻¹ and C=O stretch at 1620 cm⁻¹ provide evidence for carboxylic functional groups in the CDs. The vibration bands at 1532 and 1060 cm⁻¹ are assigned to N-H bending and C-N stretching, respectively, which shows the presence of plenty of amino groups on the srafce of the CDs. The observation can be associated with the presence of both carboxylic and amine groups in the precursor itself. Similarly, BCD-DFMO shows a wide O-H stretch band between 3000 and 3500 cm⁻¹ and the presence of a C=O stretch at 1570 cm⁻¹, which indicates the presence of a COOH functional group on the surface. Furthermore, the spectrum for DFMO drug, itself, shows a N-H stretch at 3374 cm⁻¹, an O-H stretch at 3015 cm⁻¹, and a C=O stretch at 1635 cm⁻¹ to indicate both amine and carboxylic functional groups in the molecule. Elemental analysis of the DFMO carbon dots revealed composition for C, H, O, and N to be 45.54, 4.88, 7.58, and 10.39%, respectively. The remaining 31.61% can be attributed to a F atom obtained from the DFMO precursor. The highly positive charge of DFMO CDs can be attributed to the abundance of primary amine groups on their surfaces. This can be supported by the zeta potential measurement of DFMO CDs, which was +34.7 mV. This high positive charge can be attributed to the abundance of primary amine groups.

The morphology and size distribution of the DFMO CDs were characterized using AFM and TEM images (Figure 3a,b). AFM images provide the height in the z dimension, whereas TEM gives measurements in the x and y dimensions. Sonication was done for 30 min before images were taken to prevent particle

ACS Applied Bio Materials www.acsabm.org Article

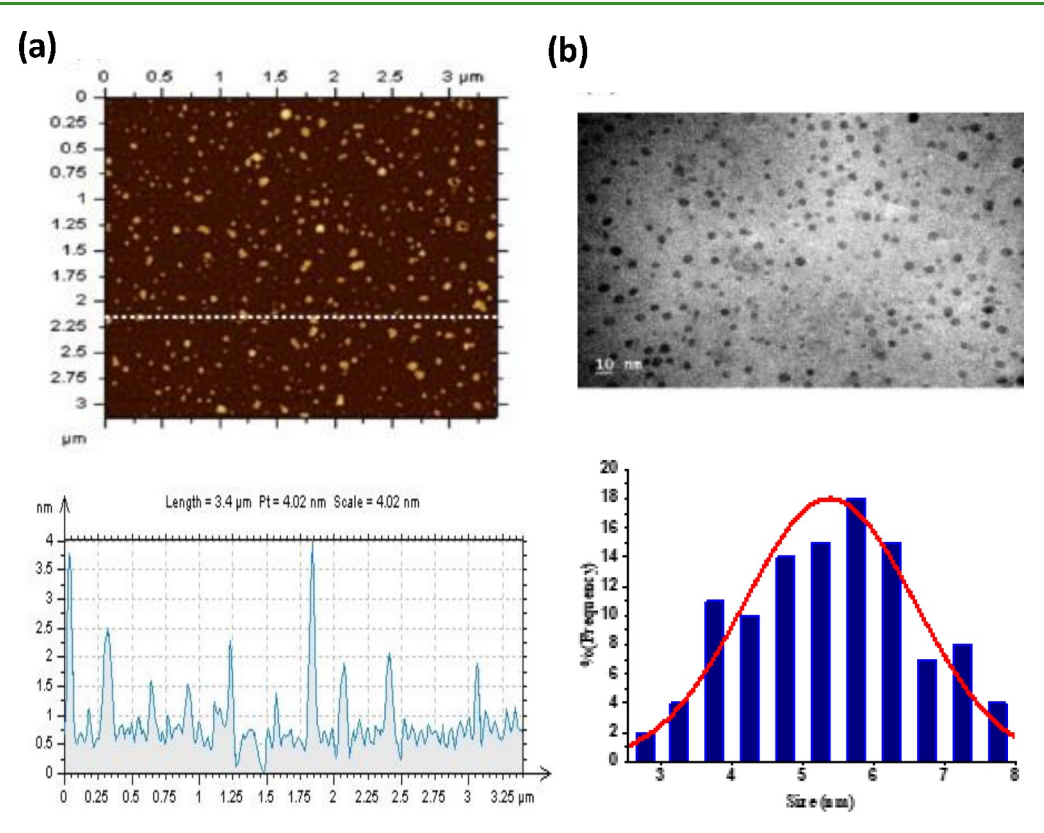


Figure 3. (a) AFM picture and profile of DFMO CDs. The white dotted line on the AFM image shows the height profile of the particle at z dimension, which was 4 nm for the tallest particle. (b) TEM image followed by a DFMO CDs histogram fitted with Gaussian size distribution. The scale bar used is 10 nm (n > 300).

aggregation. AFM images of the DMFO CDs showed a mean height of 4 nm. TEM showed a wider distribution in the range of 3 to 7 nm. Therefore, the size average was determined to be approximately 4–5 nm according to the measurements of more than 300 CDs.

The XRD pattern of synthesized DFMO CDs (Figure 4) shows the diffraction peak is centered at $2\theta = 23^{\circ}$, and d spacing = 0.355 nm. The 2θ peak at 23° for the DFMO CDs shows that the synthesized CDs are graphitic in nature with graphitic carbon (001) crystal planes.³⁸

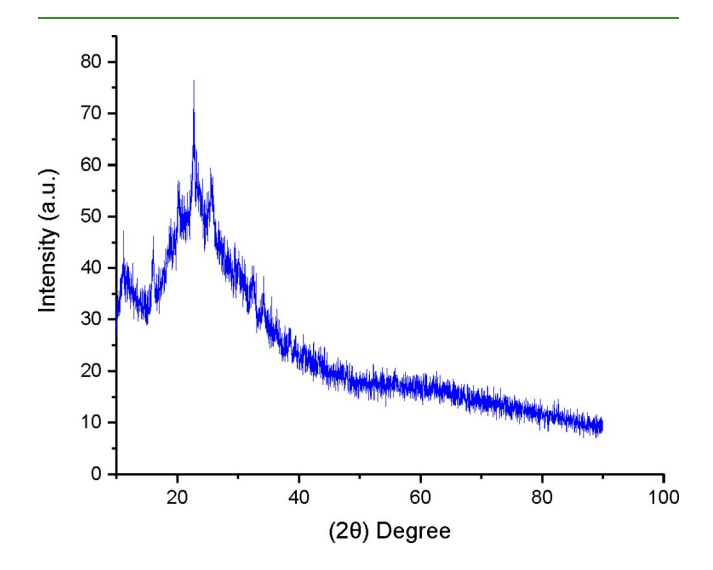


Figure 4. XRD pattern for DFMO CDs.

Comparing Cytotoxicity of Conventional DFMO, DFMO CDs, and BCD-DFMO Conjugate. Here, we selected two NB cell lines, N-MYC-amplified line SMS-KCNR and non-N-MYC-amplified line SK-N-AS, to undergo treatment with the three experimental groups. These cell lines were treated with different concentrations of conventional DFMO from $10 \mu M$ to 30 mM, our novel DFMO CDs from $100 \text{ to } 500 \mu M$, as well as black carbon dots conjugated to DFMO from $100 \text{ to } 500 \mu M$ (Figure 5a,b). In both cell lines, traditional DFMO alone reduced viability to \sim 60% or less survival rate at concentrations $\geq 1 \text{ mM}$, which is comparable with previously published work.³⁹

Our new CDs synthesized from conventional DFMO were then used to treat the same cell lines as above. Our CDs were found to induce a dose-dependent decrease in cell viability in both cell lines at dramatically lower concentrations. When compared with traditional DFMO, lower concentrations of DFMO CDs were required to achieve comparable losses of cell viability. The IC₅₀ for DFMO was 33.95 \pm 9.5 and 4.61 \pm 0.14 mM for SK-N-AS and SMS-KCNR, respectively. In contrast, the IC_{50} for our DFMO CDs was 0.65 ± 0.13 and 0.13 ± 0.02 mM for SK-N-AS and SMS-KCNR, respectively. As shown in Figure 4, in non-N-MYC-amplified SK-N-AS cells, 500 μ M of our DFMO CDs was comparable to 30 mM of the DFMO traditionally used to treat patients. Most significantly, in the more aggressive N-MYC-amplified SMS-KCNR line, a concentration of 30 mM of clinically utilized DFMO resulted in a decrease of \sim 60% cell viability, whereas 500 μ M of our DFMO CDs was able to induce a dramatic ~80% reduction in cell

SMS-KCNR cells are prognostically more challenging to treat because of N-MYC amplification and subsequent ornithine decarboxylase overexpression. Notably, 30 mM of conventional

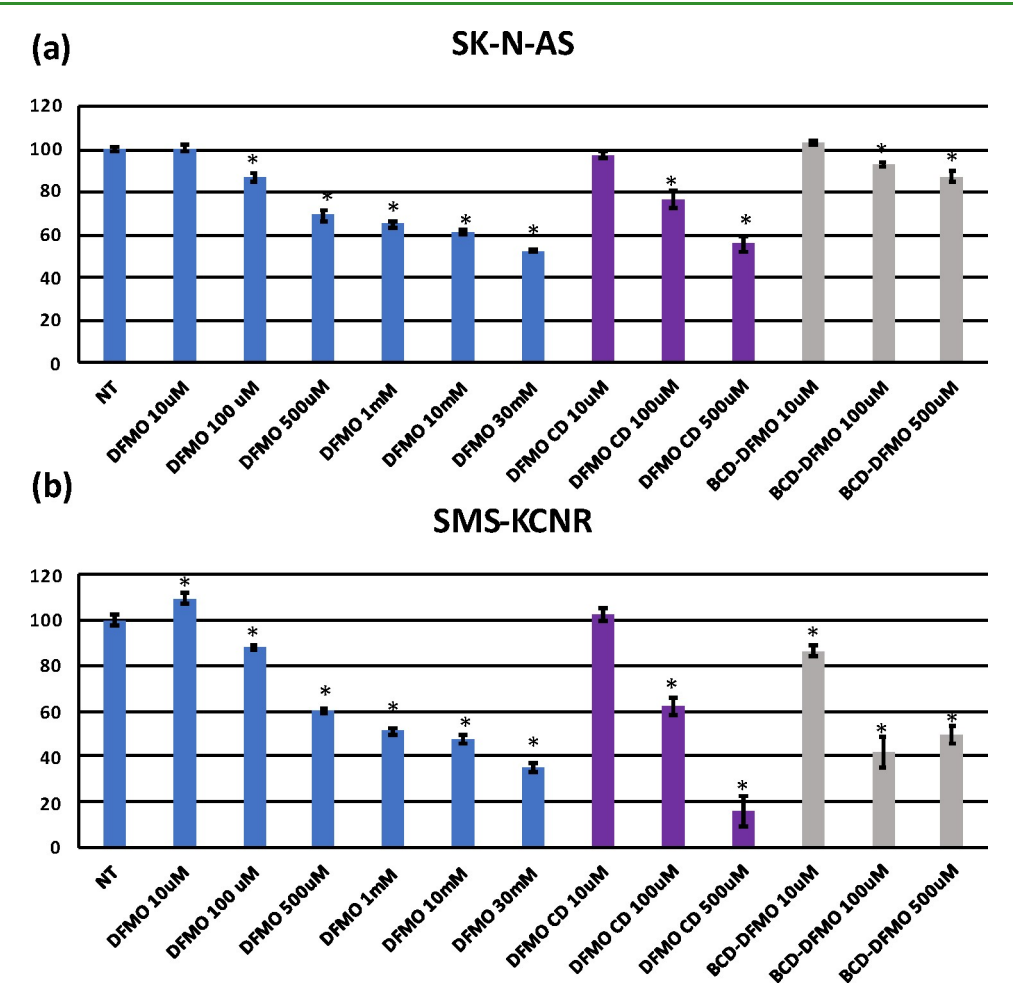


Figure 5. (a) Cytotoxicity study of conventional DFMO, DFMO carbon dots, and DFMO conjugated to black carbon dots on cell line SMS-KCNR. (b) Cytotoxicity study of conventional DFMO, DFMO carbon dots, and DFMO conjugated to black carbon dots on cell line SK-N-AS. Results are presented as % viable cells. *p < 0.05 in comparison with nontreated control.

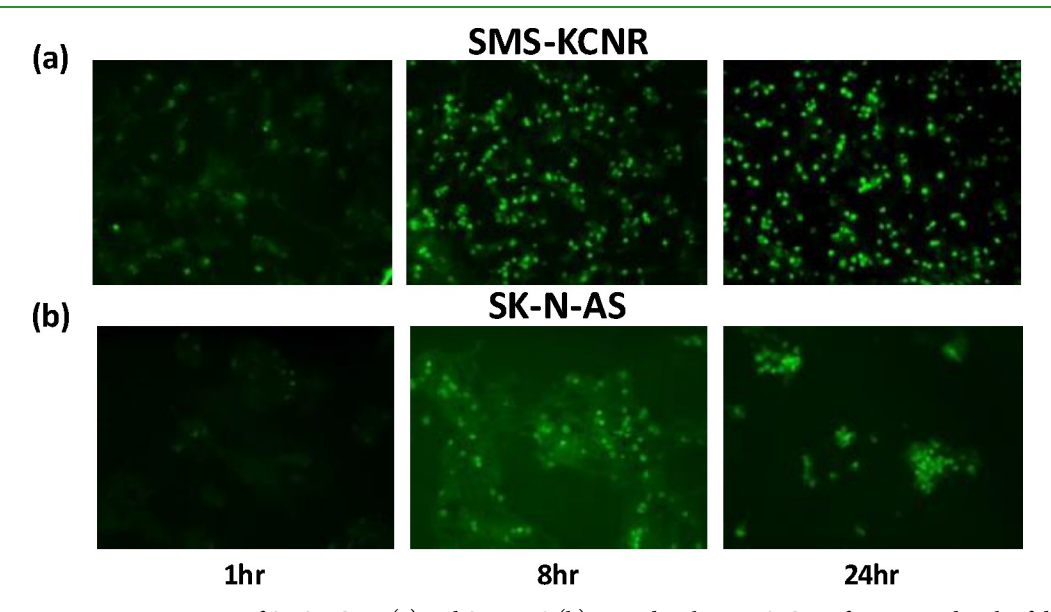


Figure 6. Fluorescenc microscopy images of SMS-KCNR (a) and SK-N-AS (b) treated with DFMO CDs after 1, 8, and 24 h of drug exposure.

DFMO was less cytotoxic than a 60-fold lower dose, 500 μ M, of DFMO CDs. This suggests that neuroblastoma cell lines are much more sensitive to DFMO CDs than to the DFMO commonly used clinically.

The effect of clinically utilized DFMO was further studied by conjugating it with well-studied nontoxic black carbon dots (BCD) via amide linkage to synthesize a BCD-DFMO conjugate. The BCD-DFMO conjugate was found to induce

ACS Applied Bio Materials www.acsabm.org Article

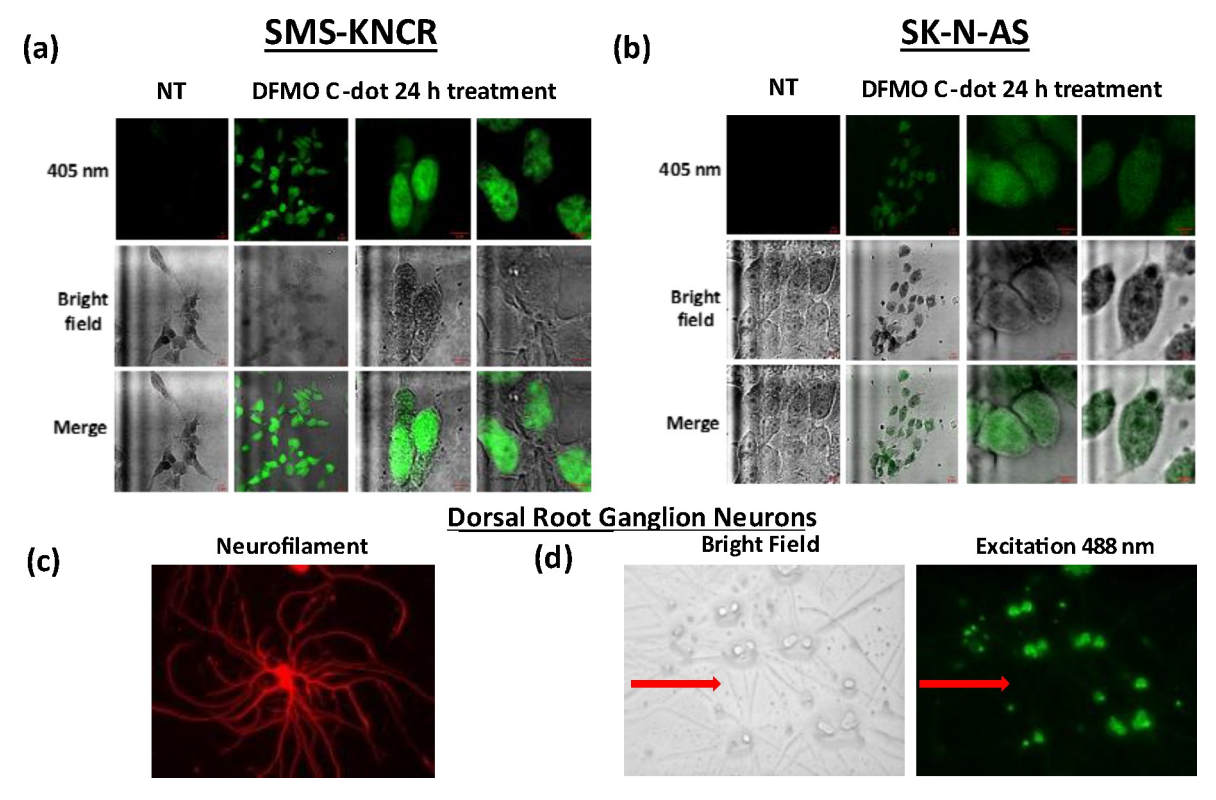


Figure 7. (a) Fluorescenc microscopy green, bright channel, and merged images of SMS-KCNR (a) and SK-N-AS (b) after 24 h of exposure to DFMO CDs. (c) Neurofilament staining of a DRG neuronal cell culture. (d) Fluorescence microscopy green and bright channel images of dorsal root ganglion neurons after 24 h of exposure to DFMO CDs. Red arrows (with scale of 30 μ m) point to neuronal axons.

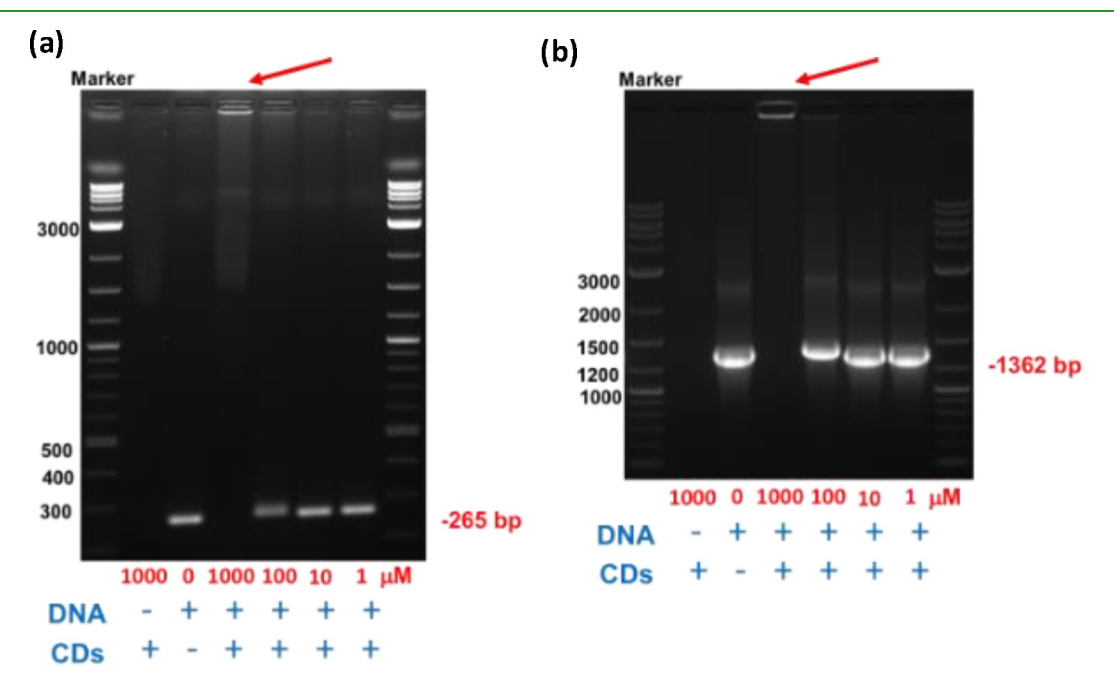


Figure 8. (a) Agarose gel electrophoresis showing the interaction of CDs with 265 bp DNA for 100 min and (b) with 1362 bp DNA for 100 min. The concentration of CDs is shown in μ M.

cell death at a level comparable with that of DFMO alone. The highest concentration of 500 μ M of BCD-DFMO conjugation was not able to induce the drastic increase in cell death exhibited in both cell lines as evidenced with treatment of 500 μ M of DFMO CDs. Taken together, DFMO CDs are much more effective than both free DFMO drug and BCD-DFMO conjugates in reducing NB cell viability. The effect of this

therapy is more dramatic in high-risk N-MYC-amplified NB cells.

In Vitro Bioimaging. The biodistribution of CDs inside cells was studied by treating NB cells with synthesized DFMO CDs, and fluorescence images were taken after 1, 8, and 24 h of treatment (Figure 6a,b).

Within 1 h of treatment, the CDs could be observed in the cells. Initially, the fluorescence signal was distributed homogeneously throughout the cells, which indicates that the CDs may be diffusing through the cell membrane. The PL is much more prominent at 8 h when juxtaposed with the 1 and 24 h time points, which suggests that DFMO CDs enter cells, disperse themselves, and are then removed from the cell over time via an unknown process. At 24 h, the CDs can be seen predominantly localized to the nucleus, though the cytoplasm can still be seen emitting low levels of fluorescence (Figure 7a,b). The biodistribution of DFMO CDs in nontumor dorsal root ganglion (DRG) neurons was analyzed after 24 h exposure. The DRG neurons contain a cell body where the nucleus is located, with axons radiating outward, as shown in Figure 7c. In the treated DRG cells, DFMO CD localization to the nucleus is evident by the hyperintense signal emitted from the cell bodies paired with the minimal fluorescence along axons (Figure 7d, red arrows).

We hypothesize that DFMO CD localization to the nucleus can be attributed to the presence of fluorine atoms present in DFMO, as previous studies have shown that the presence of fluorine increases the nucleus-targeting capability of CDs. 40 Conversely, the many positive charges of surface moieties on DFMO may be attracted to the predominantly negatively charged DNA in the nucleus. The zeta potential of DFMO CDs was found to be +34.7 mV. It follows that there may be nuclear attraction because the nuclear membrane has a potential of -15 mV. Here, we show that DFMO CDs initially distribute themselves throughout the cell body and localize themselves to the nucleus over time.

Interaction of DFMO CDs with DNA. The mechanism by which our DFMO CDs localized to the nucleus and induced losses in cell viability was further investigated by testing the possibility of DFMO CDs interacting directly with DNA. Since DNA is negatively charged, it is feasible that our positively charged DFMO CDs could bind to DNA. This was tested by incubating DFMO CDs with DNA prior to agarose gel electrophoresis. At the highest concentration (1000 μ M), the DFMO CDs blocked most of the DNA from running into the gel (red arrows), although a smear can be seen with the smallersized DNA, i.e., the 265 bp (Figure 8a), which suggests a possibly hetrogeneous mix of DFMO CDs bound to DNA. At 100 μ M, and to some degree with the lower concentrations, a "increase in size" or shift in DNA can be observed with both sizes of DNA (Figure 8a,b), thereby indicating that the DFMO CDs retarded the mobility of the DNA. Taken together, this data suggests that the DFMO CDs directly and strongly interact with the DNA, most likely by electrostatic interactions.

4. DISCUSSION

DFMO is currently used as one of the drugs for maintenance therapy to avoid relapse in high-risk NB cases. ⁴¹ It is an irreversible inhibitor of ornithine decarboxylase (ODC), the rate-limiting enzyme in polyamine synthesis. ⁸ It has been shown that NB tumors display an elevated level of ODC and polyamine content. This is particularly true in high-risk NBs with N-MYC amplification. Therefore, DFMO use in *in vitro* and *in vivo* xenograft model studies have shown a reduction of tumor proliferation. ^{42,43} Furthermore, studies have shown that NB cells treated with DFMO at concentrations >1000 μ M experience proliferation arrest, and cells treated with concentrations ranging from 150 to 500 μ M experience a reduction in colony formation. ⁴⁴

Here, we show that DFMO drug, itself, can be used as a substrate to generate carbon-dot nanoparticles using a "topdown" approach. These DFMO CDs at much lower concentrations were able to exert reductions in cell viability comparable with high-dose DFMO. Consistent with previous findings asserting that traditional DFMO tends to work best in aggressive N-MYC-amplified tumors, N-MYC-amplified SMS-KCNR demonstrated a more drastic loss of cell viability than did non-N-MYC-amplified SK-N-AS. Though results were more dramatic in SMS-KCNR, the DFMO CDs significantly outperformed DFMO alone in both cell lines. In SK-N-AS, the IC₅₀ for DFMO CDs was 52 times lower than that of traditional DFMO. In SMS-KCNR, the IC₅₀ for the DFMO CDs was 36 times lower than conventional DFMO. Though the BCD-DFMO conjugates significantly reduced cell viability in both lines, they were not as effective as the novel DFMO CDs. We postulate that the retention of traditional DFMO on the BCD-DFMO conjugates explains why similar results were observed between DFMO alone and the conjugates. The DFMO CDs were shown to localize to the cell nucleus, fluoresce, and interact with DNA once there.

This technology has broad implications for oncologic therapeutics developed in the future. This project serves as a proof of concept, showing that antineoplastic drugs conventionally used at the bedside today may have untapped potential in the form of carbon-dot transformation. Here, we demonstrate that DFMO CDs at drastically lower concentrations can exert the same effect as their "parent drug" counterparts, leading to potentially fewer side-effects and peripheral toxicity—a limiting factor in many chemotherapeutic treatment regiments. These novel CDs also bind to DNA and fluoresce, suggesting that they may have a role in imaging, as is routine with MIBG scanning or 5-ALA utilization in glioma resection. 45,46 Further studies should aim to explore the translatability of this technology to in vivo models by establishing safety profiles, DFMO CD optimization, and conjugation with ligands to target tumorspecific antigens such as GD2. Further studies are needed to understand the impact DFMO CDs may have when implemented into multimodal treatment approaches for NB in the future.

5. CONCLUSION

In summary, we successfully prepared new chemotherapeutic carbon dots (DFMO CDs) from conventionally used DFMO via a solvothermal "top-down" method. Characteristics of the DFMO CDs were determined using standard spectroscopic and advanced imaging techniques. Cytotoxicity studies of the DFMO CDs were performed using two neuroblastoma cell lines, N-MYC-amplified SMS-KCNR and non-N-MYC-amplified SK-N-AS. DFMO CDs displayed a dramatic advantage over traditional DFMO alone because they required an over 60-fold lower concentration to produce comparable losses in viability at 30 mM and 500 μ M of DFMO and DFMO CDs, respectively. The uptake and distribution of the DFMO CDs were studied using bioimaging of both neuroblastoma cells and dorsal root ganglia neurons. The images revealed that DFMO CDs have nucleus targeting ability. Agarose gel electrophoresis revealed significant binding and interaction between DFMO CD and DNA. This work reflects the potential of CDs as theranostic agents with the capability to increase cell death at lower concentrations. Further investigation is warranted to fully appreciate the clinical translatability of this technology.

AUTHOR INFORMATION

Corresponding Authors

Roger M. Leblanc — Department of Chemistry, University of Miami, Coral Gables, Florida 33146, United States; orcid.org/0000-0001-8836-8042; Email: rleblanc@miami.edu

Regina M. Graham — Department of Chemistry, University of Miami, Coral Gables, Florida 33146, United States; University of Miami Brain Tumor Initiative, Department of Neurosurgery, University of Miami Miller School of Medicine, Miami, Florida 33136, United States; Sylvester Comprehensive Cancer Center, University of Miami Health System, Miami, Florida 33136, United States; Email: rgraham@med.miami.edu

Authors

Suraj Paudyal – Department of Chemistry, University of Miami, Coral Gables, Florida 33146, United States

Frederic Anthony Vallejo — Department of Neurosurgery, University of Miami Miller School of Medicine, Miami, Florida 33136, United States; University of Miami Brain Tumor Initiative, Department of Neurosurgery, University of Miami Miller School of Medicine, Miami, Florida 33136, United States

Emel Kirbas Cilingir – Department of Chemistry, University of Miami, Coral Gables, Florida 33146, United States

Yiqun Zhou – Department of Chemistry, University of Miami, Coral Gables, Florida 33146, United States

Keenan J. Mintz – Department of Chemistry, University of Miami, Coral Gables, Florida 33146, United States

Yelena Pressman — The Miami Project to Cure Paralysis, University of Miami Miller School of Medicine, Miami, Florida 33136, United States

Jun Gu – Department of Chemistry, University of Miami, Coral Gables, Florida 33146, United States

Steven Vanni — Department of Neurosurgery, University of Miami Miller School of Medicine, Miami, Florida 33136, United States; HCA Florida University Hospital, Davie, Florida 33328, United States; Department of Medicine, Dr. Kiran C. Patel College of Allopathic Medicine, Davie, Florida 33328, United States

Complete contact information is available at: https://pubs.acs.org/10.1021/acsabm.2c00309

Author Contributions

These authors contributed equally.

Notes

The authors declare no competing financial interest.

ACKNOWLEDGMENTS

We would like to thank our wonderful laboratory volunteers: Wildlif Bayard, Meghana Sankaran, Athina Yoham, and Carolina Matta. R.M.L. acknowledges the support of the National Science Foundation under the grants 1809060 and 2041413. R.M.G. acknowledges the support of the Mystic Force Foundation and Florida department of health (grant 21L08).

ABBREVIATIONS

NB, neuroblastoma; CDs, carbon dots; DFMO, difluormethylornithine; BCDs, black carbon dots; DRG, dorsal root ganglion

REFERENCES

- (1) Maris, J. M. Recent advances in neuroblastoma. N. Engl. J. Med. **2010**, 362, 2202–2211.
- (2) Huang, M.; Weiss, W. A. Neuroblastoma and MYCN. *Cold Spring Harbor Perspect. Med.* **2013**, 3, a014415.
- (3) Maris, J. M.; Hogarty, M. D.; Bagatell, R.; Cohn, S. L. Neuroblastoma Lancet 2007, 369, 2106–2120.
- (4) Kaczówka, P.; Wieczorek, A.; Czogała, M.; Książek, T.; Szewczyk, K.; Balwierz, W. J. C. O. The role of N-Myc gene amplification in neuroblastoma childhood tumour-single-centre experience. *Wspolczesna Onkol.* **2018**, *22*, 223–228.
- (5) Hudson, M. M.; Mertens, A. C.; Yasui, Y.; Hobbie, W.; Chen, H.; Gurney, J. G.; Yeazel, M.; Recklitis, C. J.; Marina, N.; Robison, L. R.; Oeffinger, K. C. Childhood Cancer Survivor Study, I. Health status of adult long-term survivors of childhood cancer: a report from the Childhood Cancer Survivor Study. *JAMA* 2003, 290, 1583—92.
- (6) Sholler, G. L. S.; Ferguson, W.; Bergendahl, G.; Bond, J. P.; Neville, K.; Eslin, D.; Brown, V.; Roberts, W.; Wada, R. K.; Oesterheld, J.; Mitchell, D.; Foley, J.; Parikh, N. S.; Eshun, F.; Zage, P.; Rawwas, J.; Sencer, S.; Pankiewicz, D.; Quinn, M.; Rich, M.; Junewick, J.; Kraveka, J. M. Maintenance DFMO Increases Survival in High Risk Neuroblastoma. *Sci. Rep* **2018**, *8*, 14445.
- (7) Bassiri, H.; Benavides, A.; Haber, M.; Gilmour, S. K.; Norris, M. D.; Hogarty, M. D. Translational development of difluoromethylornithine (DFMO) for the treatment of neuroblastoma. *Transl. Pediatr.* **2015**, *4*, 226–238.
- (8) Meyskens, F. L.; Gerner, E. W. Development of difluoromethylornithine (DFMO) as a chemoprevention agent. *Clin. Cancer Res.* **1999**, *5*, 945–951.
- (9) Tao, H.; Yang, K.; Ma, Z.; Wan, J.; Zhang, Y.; Kang, Z.; Liu, Z. J. S. In vivo NIR fluorescence imaging, biodistribution, and toxicology of photoluminescent carbon dots produced from carbon nanotubes and graphite. *Small* **2012**, *8*, 281–290.
- (10) Chen, N.; He, Y.; Su, Y.; Li, X.; Huang, Q.; Wang, H.; Zhang, X.; Tai, R.; Fan, C. The cytotoxicity of cadmium-based quantum dots. *Biomaterials* **2012**, *33*, 1238–1244.
- (11) Li, J. J.; Zou, L.; Hartono, D.; Ong, C. N.; Bay, B. H.; Lanry Yung, L. Gold nanoparticles induce oxidative damage in lung fibroblasts in vitro. *Adv. Mater.* **2008**, *20*, 138–142.
- (12) Napierska, D.; Thomassen, L. C.; Lison, D.; Martens, J. A.; Hoet, P. The nanosilica hazard: another variable entity. *Particle and fibre toxicology* **2010**, *7*, 39.
- (13) Lau, J.; Lin, K. S.; Benard, F. Past, Present, and Future: Development of Theranostic Agents Targeting Carbonic Anhydrase IX. *Theranostics* **2017**, *7*, 4322–4339.
- (14) Ma, Z.; Wan, H.; Wang, W.; Zhang, X.; Uno, T.; Yang, Q.; Yue, J.; Gao, H.; Zhong, Y.; Tian, Y.; Sun, Q.; Liang, Y.; Dai, H. A theranostic agent for cancer therapy and imaging in the second near-infrared window. *Nano Res.* **2019**, *12*, 273–279.
- (15) Luo, S.; Yang, X.; Shi, C. Newly Emerging Theranostic Agents for Simultaneous Cancertargeted Imaging and Therapy. *Curr. Med. Chem.* **2016**, 23, 483–497.
- (16) Sarkar, B.; Paira, P. Theranostic Aspects: Treatment of Cancer by Nanotechnology. *Mini Rev. Med. Chem.* **2018**, *18*, 969–975.
- (17) Yao, J.; Yang, M.; Duan, Y. Chemistry, biology, and medicine of fluorescent nanomaterials and related systems: new insights into biosensing, bioimaging, genomics, diagnostics, and therapy. *Chem. Rev.* **2014**, *114*, 6130–6178.
- (18) Jaque, D.; Maestro, L. M.; Del Rosal, B.; Haro-Gonzalez, P.; Benayas, A.; Plaza, J.; Rodriguez, E. M.; Sole, J. Nanoparticles for photothermal therapies. *Nanoscale* **2014**, *6*, 9494–9530.
- (19) Lucky, S. S.; Soo, K. C.; Zhang, Y. Nanoparticles in photodynamic therapy. *Chem. Rev.* **2015**, *115*, 1990–2042.
- (20) Pastorin, G. Crucial functionalizations of carbon nanotubes for improved drug delivery: a valuable option? *Pharm. Res.* **2009**, 26, 746–769
- (21) Derfus, A. M.; Chan, W. C.; Bhatia, S. N. Probing the cytotoxicity of semiconductor quantum dots. *Nano Lett.* **2004**, *4*, 11–18.

- (22) Cheng, L.; Yang, K.; Shao, M.; Lu, X.; Liu, Z. In vivo pharmacokinetics, long-term biodistribution and toxicology study of functionalized upconversion nanoparticles in mice. Nanomed. J. 2011, 6 (8), 1327-1340.
- (23) Tang, J.; Kong, B.; Wu, H.; Xu, M.; Wang, Y.; Wang, Y.; Zhao, D.; Zheng, G. Carbon nanodots featuring efficient FRET for real-time monitoring of drug delivery and two-photon imaging. J. Adv. Mater. **2013**, 25, 6569–6574.
- (24) Liyanage, P. Y.; Zhou, Y.; Al-Youbi, A. O.; Bashammakh, A. S.; El-Shahawi, M. S.; Vanni, S.; Graham, R. M.; Leblanc, R. M. Pediatric glioblastoma target-specific efficient delivery of gemcitabine across the blood-brain barrier via carbon nitride dots. Nanoscale 2020, 12, 7927-
- (25) Li, J.; Li, M.; Tian, L.; Qiu, Y.; Yu, Q.; Wang, X.; Guo, R.; He, Q. Facile strategy by hyaluronic acid functional carbon dot-doxorubicin nanoparticles for CD44 targeted drug delivery and enhanced breast cancer therapy. Int. J. Pharm. 2020, 578, 119122-119136.
- (26) Pardo, J.; Peng, Z.; Leblanc, R. M. Cancer Targeting and Drug Delivery Using Carbon-Based Quantum Dots and Nanotubes. Molecules 2018, 23, 378-398.
- (27) Hettiarachchi, S. D.; Graham, R. M.; Mintz, K. J.; Zhou, Y.; Vanni, S.; Peng, Z.; Leblanc, R. M. Triple conjugated carbon dots as a nano-drug delivery model for glioblastoma brain tumors. Nanoscale 2019, 11, 6192-6205.
- (28) Li, S.; Amat, D.; Peng, Z.; Vanni, S.; Raskin, S.; De Angulo, G.; Othman, A. M.; Graham, R. M.; Leblanc, R. M. Transferrin conjugated nontoxic carbon dots for doxorubicin delivery to target pediatric brain tumor cells. Nanoscale 2016, 8, 16662-16669.
- (29) Cilingir, E. K.; Seven, E. S.; Zhou, Y.; Walters, B. M.; Mintz, K. J.; Pandey, R. R.; Wikramanayake, A. H.; Chusuei, C. C.; Vanni, S.; Graham, R. M.; Leblanc, R. M. Metformin derived carbon dots: Highly biocompatible fluorescent nanomaterials as mitochondrial targeting and blood-brain barrier penetrating biomarkers. J. Colloid Interface Sci. **2021**, 592, 485-497.
- (30) Zhou, Y.; ElMetwally, A. E.; Chen, J.; Shi, W.; Cilingir, E. K.; Walters, B.; Mintz, K. J.; Martin, C.; Ferreira, B. C.; Zhang, W.; Hettiarachchi, S. D.; et al. Gel-like carbon dots: A high-performance future photocatalyst. J. Colloid Interface Sci. 2021, 599, 519-532.
- (31) Graham, R. M.; Hernandez, F.; Puerta, N.; De Angulo, G.; Webster, K. A.; Vanni, S. Resveratrol augments ER stress and the cytotoxic effects of glycolytic inhibition in neuroblastoma by downregulating Akt in a mechanism independent of SIRT1. Exp. Mol. Med. 2016, 48, e210.
- (32) Plant, G. W.; Currier, P. F.; Cuervo, E. P.; Bates, M. L.; Pressman, Y.; Bunge, M. B.; Wood, P. M. Purified adult ensheathing glia fail to myelinate axons under culture conditions that enable Schwann cells to form myelin. J. Neurosci. 2002, 22, 6083-91.
- (33) Li, H.; Kang, Z.; Liu, Y.; Lee, S. T. Carbon nanodots: synthesis, properties and applications. J. Mater. Chem. 2012, 22, 24230-24253.
- (34) Li, S.; Aphale, A. N.; Macwan, I. G.; Patra, P. K.; Gonzalez, W. G.; Miksovska, J.; Leblanc, R. M. Graphene oxide as a quencher for fluorescent assay of amino acids, peptides, and proteins. ACS Appl. Mater. Interfaces 2012, 4, 7069-7075.
- (35) Chen, D.; Gao, H.; Chen, X.; Fang, G.; Yuan, S.; Yuan, Y. Excitation-independent dual-color carbon dots: surface-state controlling and solid-state lighting. ACS Photonics 2017, 4, 2352–2358.
- (36) Zhao, Y.; Ou, C.; Yu, J.; Zhang, Y.; Song, H.; Zhai, Y.; Tang, Z.; Lu, S. Interfaces, Facile synthesis of water-stable multicolor carbonized polymer dots from a single unconjugated glucose for engineering white light-emitting diodes with a high color rendering index. ACS Appl. Mater. 2021, 13, 30098-30105.
- (37) Mintz, K. J.; Cilingir, E. K.; Nagaro, G.; Paudyal, S.; Zhou, Y.; Khadka, D.; Huang, S.; Graham, R. M.; Leblanc, R. M. Development of Red-Emissive Carbon Dots for Bioimaging through a Building Block Approach: Fundamental and Applied Studies. Bioconjugate Chem. 2022, 33, 226-237.
- (38) Yang, X.; Sui, L.; Wang, B.; Zhang, Y.; Tang, Z.; Yang, B.; Lu, S. Red-emitting, self-oxidizing carbon dots for the preparation of white

- LEDs with super-high color rendering index. Science China Chemistry 2021, 64, 1547-1553.
- (39) Geck, R. C.; Foley, J. R.; Murray Stewart, T.; Asara, J. M.; Casero, R. A., Jr.; Toker, A. Inhibition of the polyamine synthesis enzyme ornithine decarboxylase sensitizes triple-negative breast cancer cells to cytotoxic chemotherapy. J. Biol. Chem. 2020, 295, 6263-6277.
- (40) Gao, P.; Liu, S.; Su, Y.; Zheng, M.; Xie, Z. Fluorine-Doped Carbon Dots with Intrinsic Nucleus-Targeting Ability for Drug and Dye Delivery. Bioconjugate Chem. 2020, 31, 646-655.
- (41) Sholler, G. L. S.; Ferguson, W.; Bergendahl, G.; Bond, J. P.; Neville, K.; Eslin, D.; Brown, V.; Roberts, W.; Wada, R. K.; Oesterheld, J.; et al. Maintenance DFMO increases survival in high risk neuroblastoma. Sci. Rep. 2018, 8, 14445.
- (42) Samal, K.; Zhao, P.; Kendzicky, A.; Yco, L. P.; McClung, H.; Gerner, E.; Burns, M.; Bachmann, A. S.; Sholler, G. AMXT-1501, a novel polyamine transport inhibitor, synergizes with DFMO in inhibiting neuroblastoma cell proliferation by targeting both ornithine decarboxylase and polyamine transport. Int. J. Cancer 2013, 133, 1323-
- (43) Hogarty, M. D.; Norris, M. D.; Davis, K.; Liu, X.; Evageliou, N. F.; Hayes, C. S.; Pawel, B.; Guo, R.; Zhao, H.; Sekyere, E.; et al. ODC1 is a critical determinant of MYCN oncogenesis and a therapeutic target in neuroblastoma. Cancer Res. 2008, 68, 9735-9745.
- (44) Wallick, C. J.; Gamper, I.; Thorne, M.; Feith, D. J.; Takasaki, K. Y.; Wilson, S. M.; Seki, J. A.; Pegg, A. E.; Byus, C. V.; Bachmann, A. S. Key role for p27 Kip1, retinoblastoma protein Rb, and MYCN in polyamine inhibitor-induced G 1 cell cycle arrest in MYCN-amplified human neuroblastoma cells. Oncogene 2005, 24, 5606-5618.
- (45) Hadjipanayis, C. G.; Widhalm, G.; Stummer, W. What is the Surgical Benefit of Utilizing 5-Aminolevulinic Acid for Fluorescence-Guided Surgery of Malignant Gliomas? Neurosurgery 2015, 77, 663-
- (46) Sharp, S. E.; Trout, A. T.; Weiss, B. D.; Gelfand, M. MIBG in Neuroblastoma Diagnostic Imaging and Therapy. Radiographics 2016, 36, 258-78.

□ Recommended by ACS

Carbon Dots in Biomedicine: A Review

Peide Zhu, Dixian Luo, et al.

APRIL 20, 2022 ACS APPLIED BIO MATERIALS

READ **Z**

Red-Emissive Ruthenium-Containing Carbon Dots for Bioimaging and Photodynamic Cancer Therapy

Liangliang Yue, Xunjin Zhu, et al.

JANUARY 03, 2020

ACS APPLIED NANO MATERIALS

READ C

Copper-Doped Carbon Dots for Optical Bioimaging and **Photodynamic Therapy**

Jingmin Wang, Hong Bi, et al.

SEPTEMBER 26, 2019

INORGANIC CHEMISTRY

READ **C**

Self-Targeting Carbon Quantum Dots for Peroxynitrite Detection and Imaging in Live Cells

Yan Bai, Chengzhi Huang, et al.

DECEMBER 03, 2021

ANALYTICAL CHEMISTRY

READ **'**

Get More Suggestions >